IOWA STATE UNIVERSITY
Digital Repository

2010

Contribution to individual blazar spectrum from the cascade of very-high energy gamma rays

Ke Fang
Iowa State University

Follow this and additional works at: http://lib.dr.iastate.edu/etd

Part of the Physics Commons

Contribution to individual blazar spectrum

from the cascade of very-high energy gamma rays

by

Ke Fang

A thesis submitted to the graduate faculty

in partial fulfillment of the requirements for the degree of

MASTER OF SCIENCE

Major: Astrophysics

Program of Study Committee:
Frank Krennrich, Major Professor
Curt Struck
Kerry Whisnant
Paul Sacks

Iowa State University

Ames, Iowa

2010

DEDICATION

I would like to dedicate this thesis to my parents Shaojin Fang and Zhuoer Ke without whose support I would not have been able to complete this work. I would also like to thank Prof. Martin Pohl for his enlightening guidence and help to my entire research in ISU.

TABLE OF CONTENTS

LIST OF TABLES

v

LIST OF FIGURES

ABSTRACT

As Very High Energy (VHE) photons travel through the extragalactic background light (EBL), they will interact and generate electron and positron pairs via pair production. The newly produced electrons and positrons will Inverse-Compton scatter the background soft photons to secondary gamma-rays in the process of electromagnetic cascading. The intensity of a cosmological population emitting at VHEs will be attenuated at the highest energies due to absorption and enhanced at lower energies by the resulting cascade. We calculate the cascade radiation created by VHE photons produced by blazars and investigate the effects of cascades on the observed intensity of individual blazars. We find that the cascade radiation greatly enhances the observed intensity at the observational energy range. The prominence of the resulting features depends on the intrinsic spectral index and the location of the source. We additionally calculate the cascade radiation from several sources with distinct spectral index and cosmological positions. Finally, we discuss the implications that this analysis could have for the prediction of sourse spectrum with the observational data from VERITAS and FERMI.

CHAPTER 1.   INTRODUCTION

271 gamma-ray sources were first resolved by the energetic gamma-ray experiment telescope (EGRET) aboard the Compton Gamma-ray Observatory during the 1990s, of which 93 were identified as blazars (gamma-ray loud active galactic nuclei (AGNs)). Currently, VERITAS has detected more than a dozen blazars and has discovered VHE emission from 16 blazars, including 1ES 0806+524, RGB J0710+591, W Com, PKS 1424+240, VER J0521+211, RBS 0413, 1ES 0502+675, VER J0521+211, M82, M421, M501, 1ES1959, 1ES2344, 1ES1218, 1ES0229 and 3C66A . MAGIC has seen over10 sources up to date. The Fermi Gamma-ray Space Telescope is taking data and has already identified 709 AGN, including 300 BL lacs, 296 FSRQS, 91 other type and 72 unknows.

However, the observed spectrum have huge difference from the source spectrum. Pair production happens when the VHE photons interact with soft photons and electron-positron pairs are generated in this process (Jones, F.C (1963)). Photon-photon pair production of high-energy gamma-rays on the extragalactic background light (EBL) significantly limits the distance that such gamma-rays can propagate(Gould & Schreder (1966)).

The major contributors to the soft photon flux are Cosmic background (CMB) and EBL. CMB has been extremely well studied both spectrally and spatially, and has been shown to be a very isotropic black-body spectrum. Measurements of the CMB from COBE and WMAP have been eased by the far dominance of this component over the foreground emissions by the Galaxy and interplanetary dust (IPD). In consideration of its origin in the primeval plasma at z around 1000, the evolution of this radiation in cosmic time is also determined, the photon number density n_γ scaling with z as $n_\gamma \propto (1 + z)^3$.

The EBL includes starlight at optical, ultraviolet, and near-infrared wavelengths and rera-

diated thermal dust emission at far-infrared in galaxies. At observed energies within the VERITAS energy range, photons suffer significant attenuation due to interactions with the soft photons of the EBL (Tonia M. Venters (2009)). However the measurements of EBL are not so easy. On one side, their observation is disturbed or even prevented by the intense foreground emission over most of the wavelength range, like in near-IR and mid-IR. In addition, these radiations are generated by galaxies and active nuclei (AGN) during most of the Hubble time, particularly below redshift equals 1, so that the evolution of their photon number density is a very complex function of time and frequency. Fortunately, an enormous amount of new data at all UV-optical and IR-millimetric wavelengths have been recently obtained with astronomical observatories on ground and in space to characterize such an evolution.Currently there are several plausible models of EBL that fit the observation well. We will adopt Franceschini's model (A. Franceschini.& G. Rodighiero. (2008)) in this work to calculate the optical depth via pair production.

In addition to the pair production process, the produced electron-positron pairs will participate in the inverse-compton scattering(IC) process. In the process the pairs of electrons and positrons produced will inverse Compton scatter CMB and EBL photons to high energies as secondary gamma-ray, whose energy is a bit lower than the original photons participated the absorption. These upscattered photons will again join the absorption and this EM cascade process continues until the energies of the resulting photons are low enough that pair production is no longer efficient. IC process is very important since for any cosmological population emitting VHE gamma rays, the EM cascading results in a flux suppression at the highest energies and enhancement at lower energies and hence change the spectrum to a great extent.

The IC spectrum and flux level is actually dependent on the the intensity of the intergalacticmagnetic field, B, that can deflect the pairs diluting the intrinsic emission over certain solid angle. This deflection angle is directly proportional to the magnitude of magnetic fields. In our work we assume the magnetic field to be small such that deflection is ignorable. And this assumption is favorable since as for photons with 5TeV energy, in the case when B field is of the same magnitude as what is expected for cosmological seed fields, that is magnetic field prior

compression by structure formation and associated shocks, the deflection angle is about 10^{-6}. The displacement of that order is not directly observable on account of the limited angular resolution of gamma-ray measurements; it may impose a time delay. The light travel-time difference between going straight and at an angle $\delta\theta$ from a source located at redshift 1 is 2.5days. Clearly, this is an issue when discussing rapid variability, but we may ignore it for time-integrated spectra, like analyzing VERITAS data taken over many nights.

It is interesting to look into the source spectrum of blazars. The newly updated data from FERMI and VERITAS showed a good amount of TeV hard spectrum exist and it is helpful to learn their intrinsic spectrum to see whether the hard spectrum make sense or not. Especially for a static case when the magnetic field is small and there is no or little deflection, the source spectrum gives a deep insight of radiation transportations. Moreover, individual source spectrum is fundamental during the study of collective spectrum of blazars, which is further involved in the confinement of extragalactic gamma-ray background.

Previous works have been done to predict the intrinsic spectrum via the optical depth from pair production(Krennrich, F (2008) A. Franceschini.& G. Rodighiero. (2008) Tonia M. Venters (2009) Tonia M. Venters (2010)). In this work, we further took account of the effects of Inverse-Compton scattering and evaluated the flux suppression due to the electronmagnetic cascade of VHE photons from blazars. In Section 2 we present the formalism of the calculation of the blazar intensity and a short discussion of the aspects of the code we used. In Section 3, we discuss the inputs of the calculation and their uncertainties. In Section 4, we present the results of the calculation, and we discuss these results in Section 5.

All quantities are computed in this work assuming a geometry for the Universe with $H_0 = 70 km\, s^{-1}\, Mpc^{-1}, \Omega_m = 0.3, \Omega_\Lambda = 0.7$.

CHAPTER 2.   FORMALISM

2.1   The cosmic photon-photon opacity

Once we know the redshift-dependent background photon density, the cosmic opacity for photon-photon interactions from the pair production crosssection is calculated as follows:

$$\sigma_{\gamma\gamma}(E_\gamma, \epsilon, \theta) = \frac{3\sigma_T}{16} (1 - \beta^2) \times \left[2\beta(\beta^2 - 2) + (3 - \beta^4) \ln \left(\frac{1 + \beta}{1 - \beta} \right) \right] \tag{2.1}$$

where ϵ is the energy of the background photon, E_γ that of the high-energy colliding one, σ_T the Thompson cross-section, and where the argument β should be computed as(Heitler, W., (1960)):

$$\beta \equiv (1 - 4\, m_e^2\, c^4/s)^{1/2}; \quad s \equiv 2\, E_\gamma\, \epsilon\, x\, (1 + z); \quad x \equiv (1 - \cos\theta) \tag{2.2}$$

According to the definition of optical depth, the optical depth for a high-energy photon E_γ travelling through a cosmic medium filled with low-energy photons with density $n_\gamma(z)$ from a source at z_e to an observer at the present time is:

$$\tau(E_\gamma, z_e) = c \int_0^{z_e} dz\, \frac{dt}{dz} \int_0^2 dx\, \frac{x}{2} \int_{\epsilon_{th}}^\infty d\epsilon \frac{dn_\gamma(\epsilon, z^*)}{d\epsilon}\, \sigma_{\gamma\gamma}(\beta) \tag{2.3}$$

where

$$\epsilon_{th} = \frac{2\, m_e^2\, c^4}{E_\gamma\, (1 + z)\, x} \tag{2.4}$$

For a flat universe, the differential of time to be used in eq. (2.3) is:

$$\frac{dt}{dz} = \frac{1}{H_0(1 + z)} \left[(1 + z)^2(1 + \Omega_m\, z) - z\, (z + 2)\, \Omega_\Lambda \right]^{-1/2} \tag{2.5}$$

Because we want to follow the cascading, we break down the integral into finite steps that give the optical depth for a small step in redshift, δz.

$$\delta\tau = c\, \delta z\, \frac{dt}{dz} \int_0^2 dx\, \frac{x}{2} \int_{\epsilon_{th}}^\infty d\epsilon \frac{dn_\gamma(\epsilon, z^*)}{d\epsilon}\, \sigma_{\gamma\gamma}(\beta) \tag{2.6}$$

To be careful in eliminating possible errors, we introduced two divisions of redshift bins. z_b represents the boundary bin for redshift, with data points locating at 0, 1, ..., while z_c represents the center bin with data locating at 0.5, 1.5 ....

2.2 Absorption

Let the γ-ray spectrum be

$$F(E_\gamma, z_b(i)) = dn/dE_\gamma$$

As the radiation passes through the redshift interval δz, the spectrum is changed by absorption as:

$$
\begin{aligned}
F(E_\gamma, z_b(i-1)) \quad &= F(E_\gamma, z_b(i)) \exp\left(-\delta\tau\left[z_c(i)\right]\right) \\
&\simeq F(E_\gamma, z_b(i)) \left(1 - \delta\tau\left[z_c(i)\right]\right)
\end{aligned}
\tag{2.7}
$$

where $\delta\tau$ is the optical depth for a high-energy photon E_γ travelling through a cosmic medium of extragalactic background. The square of the invariant mass-energy of the 2-photon system is given by $s = M^2\,c^4 = 2\,E_\gamma\,\epsilon\,x\,(1+z)$ where, as before, $\epsilon = \epsilon(z)$, $x = 1 - \cos\theta$, and $E_\gamma = E_\gamma(z=0)$. From that I can calculate the Lorentz factor of the CM system in the Lab frame by dividing the total energy by the mass.

$$
\gamma_{\mathrm{CM}} = \frac{E_\gamma\,(1+z) + \epsilon}{\sqrt{s}} \simeq \frac{E_\gamma\,(1+z)}{\sqrt{s}} \simeq \sqrt{\frac{E_\gamma\,(1+z)}{2\,\epsilon\,x}}
\tag{2.8}
$$

The kinetic energy available per electron or positron in the CM frame (marked with *) is the invariant mass-energy of the 2-photon system minus the rest-mass energy of the created electron-positron pair.

$$
\begin{aligned}
E_{\mathrm{kin}}^* \quad &= \quad \frac{1}{2}\left[\sqrt{s} - 2\,m_e\,c^2\right] \simeq \frac{1}{2}\left[\frac{E_\gamma\,(1+z)}{\gamma_{\mathrm{CM}}} - 2\,m_e\,c^2\right] \qquad \Rightarrow \\
\gamma^* \quad &= \quad \frac{E_\gamma\,(1+z)}{2\,\gamma_{\mathrm{CM}}\,m_e\,c^2}
\end{aligned}
\tag{2.9}
$$

The absorped energy is turned into electron-positron pairs. we know their distribution in the CM frame:

$$
f_e^*(\gamma^*) = m_e\,c^2\,\frac{dn}{dE_{\mathrm{kin}}^*\,d\cos\theta^*} = \frac{dn}{d\gamma^*\,d\cos\theta^*} = \delta\left(\gamma^* - \frac{E_\gamma\,(1+z)}{2\,\gamma_{\mathrm{CM}}\,m_e\,c^2}\right)
\tag{2.10}
$$

For a small step in redshift, the number of absorbed photons is

$$
\begin{aligned}
dN &= F(E_\gamma, z_b(i))\, \delta\tau\, [z_c(i)]\, dE_\gamma \\
&= F(E_\gamma, z_b(i))\, c\, \delta z\, \frac{dt}{dz}\, \frac{x}{2}\, \frac{dn_\gamma(\epsilon, z)}{d\epsilon}\, \sigma_{\gamma\gamma}\, dE_\gamma\, dx\, d\epsilon
\end{aligned}
\tag{2.11}
$$

We need an expression of the form $dN/d\gamma_{\mathrm{CM}}$ to describe the number of photons absorbed (= number of pairs produced) per interval of γ_{CM}. Thus we transform $x \to \gamma_{\mathrm{CM}}$. Since

$$
\gamma_{\mathrm{CM}} = \sqrt{\frac{E_\gamma\,(1+z)}{2\,\epsilon\,x}} \qquad\qquad x = \frac{E_\gamma\,(1+z)}{2\,\gamma_{\mathrm{CM}}^2\,\epsilon}
$$

For the transformation of variables we need

$$
\left|\frac{dx}{d\gamma_{\mathrm{CM}}}\right| = \frac{E_\gamma\,(1+z)}{\gamma_{\mathrm{CM}}^3\,\epsilon} \qquad\Rightarrow\qquad dx = d\gamma_{\mathrm{CM}}\left|\frac{dx}{d\gamma_{\mathrm{CM}}}\right|
$$

and thus obtain the total distribution of pair-creation events per redshift interval δz

$$
\begin{aligned}
\frac{dN}{d\gamma_{\mathrm{CM}}} =\ & c\,\delta z\,\frac{dt}{dz}\,\frac{(1+z)^2}{4\,\gamma_{\mathrm{CM}}^5}\int dE_\gamma\ F(E_\gamma, z_b(i))\, E_\gamma^2\, \Theta(E_\gamma - E_{\min}) \\
& \times \int d\epsilon\ \frac{dn_\gamma(\epsilon, z)}{d\epsilon}\,\frac{\sigma_{\gamma\gamma}}{\epsilon^2}\,\Theta(\epsilon - \epsilon_{\min})
\end{aligned}
\tag{2.12}
$$

The energy distribution of the electrons in the Lab frame is now given as $f_3(\gamma)$, where $f_2 = dN/d\gamma_{\mathrm{CM}}$ above and $f_1 = f_e^*(\gamma^*)$ as calculated above.

$$
f_3(\gamma) = \int_1^\infty d\gamma^* \int_{\gamma^-}^{\gamma^+} d\gamma_{CM}\ \frac{f_1(\gamma^*, x^*(\gamma, \gamma^*, \gamma_{CM}), \gamma_{CM})\, f_2(\gamma_{CM})}{\sqrt{(\gamma^{*2}-1)(\gamma_{CM}^2-1)}}
\tag{2.13}
$$

with

$$
\gamma^\pm = \gamma\gamma^* \pm \sqrt{(\gamma^{*2}-1)(\gamma^2-1)}
\tag{2.14}
$$

Thus we get

$$
\begin{aligned}
\delta N_e(\gamma) =\ & c\,\delta z\,\frac{dt}{dz}\,\frac{(1+z)^2}{4}\int dE_\gamma\ F(E_\gamma, z_b(i))\, E_\gamma^2 \int d\gamma_{CM}\ \frac{1}{\gamma_{\mathrm{CM}}^6\,\sqrt{\gamma^{*2}-1}} \\
& \times \int d\epsilon\ \frac{dn_\gamma(\epsilon, z)}{d\epsilon}\,\frac{\sigma_{\gamma\gamma}}{\epsilon^2}\,\Theta(\epsilon - \epsilon_{\min})\,\Theta(E_\gamma - E_{\min}) \\
& \times \Theta\left(\gamma_{\mathrm{CM}} - \gamma^-\right)\,\Theta\left(\gamma^+ - \gamma_{\mathrm{CM}}\right)
\end{aligned}
\tag{2.15}
$$

A trick here is, γ^* and γ_{cm} are dependent by eq (2.9) and thus the upper and lower limits of the integral presented in (2.13) are coupled. To decouple the upper limit,

$$\gamma^* = \frac{\gamma_{\text{max}}}{\gamma_{\text{CM}}} \qquad \Rightarrow \qquad \gamma_{\text{CM}}^2 - \gamma\,\gamma_{\text{max}} \leq \sqrt{(\gamma^2 - 1)\,(\gamma_{\text{max}}^2 - \gamma_{\text{CM}}^2)} \tag{2.16}$$

which is always fulfilled if $\gamma_{\text{CM}}^2 \leq \gamma\,\gamma_{\text{max}}$. In the more interesting case $\gamma_{\text{CM}}^2 \geq \gamma\,\gamma_{\text{max}}$ when both sides of the relation are positive, we take the square of it, yielding

$$\gamma_{\text{CM}}^4 - 2\,\gamma_{\text{CM}}^2 \left(\frac{\gamma^2 - 1}{2} + \gamma\,\gamma_{\text{max}}\right) + \gamma_{\text{max}}^2 \leq 0 \tag{2.17}$$

which is only fulfilled between the two zeros of the left-hand side of the relation. The zeros are given by

$$\gamma_{\text{CM}}^2 = \frac{\gamma^2 - 1}{2} + \gamma\,\gamma_{\text{max}} \pm \sqrt{(\gamma^2 - 1)\left[\left(\gamma_{\text{max}} + \frac{\gamma}{2}\right)^2 - \frac{1}{4}\right]} \tag{2.18}$$

In the same way we compute the lower limit of γ_{cm}. At the same time $\gamma_{\text{CM}} \geq 1$. This leads to the new limits of integration.

$$\gamma_{\text{CM}} \geq \gamma_1 = \max\left(1, \sqrt{\frac{1}{4} + \frac{\gamma_{\text{max}}}{2\,\gamma}}\right) \tag{2.19}$$

$$\gamma_{\text{CM}} \leq \gamma_2 = \min\left(\gamma_{\text{max}}, \sqrt{\gamma^2 + \frac{\gamma\,\gamma_{\text{max}}}{2}}\right) \tag{2.20}$$

The increment in the electron spectrum (eq.10) can therefore be written as

$$\delta N_e(\gamma, z_c(i)) = \quad c\,\delta z\,\frac{dt}{dz}\,\frac{(1+z)^2}{4}\int dE_\gamma\;F(E_\gamma, z_b(i))\,E_\gamma^2 \int_{\gamma_1}^{\gamma_2} d\gamma_{CM}\;\frac{\sigma_{\gamma\gamma}}{\gamma_{\text{CM}}^5\,\sqrt{\gamma_{\text{max}}^2 - \gamma_{\text{CM}}^2}}$$

$$\times \int_{\epsilon_{\text{min}}} d\epsilon\;\frac{dn_\gamma(\epsilon, z)}{d\epsilon}\,\epsilon^{-2} \tag{2.21}$$

where

$$\epsilon_{\text{min}} = \frac{E_\gamma\,(1+z)}{4\,\gamma_{\text{CM}}^2} \qquad\qquad \beta = \sqrt{1 - \frac{\gamma_{\text{CM}}^2}{\gamma_{\text{max}}^2}} \qquad\qquad \gamma_{\text{max}} = \frac{E_\gamma\,(1+z)}{2\,m_e\,c^2}$$

and $\gamma_{1,2}$ are given by equation (2.16) and (2.17).

2.3 Updating the electron spectrum

This increment in the electron spectrum is in competition with two loss processes, the first of which is the cosmological expansion. This operates on a timescale $H_0^{-1} \simeq 4 \cdot 10^{17}$ s (taken as the time from redshift 1 to redshift 0). In addition to the reduction in the density of electrons, their energy is also reduced by the redshift and energy losses by inverse-Compton scattering of CMB photons, the same process we will later use to have the electrons produce gamma rays. The energy loss rate is

$$\dot{\gamma}_{IC} = -\frac{4 \, c \, \sigma_T \, U_{\text{CMB}} \, \gamma^2}{3 \, m_e \, c^2} = -(1+z)^4 \, \gamma^2 \, (1.3 \cdot 10^{-20} \text{ s}^{-1}) \tag{2.22}$$

where the redshift-scaling of the energy density of the CMB is accounted. The lifetime of an electron against IC losses can be estimated as

$$\tau_{IC} \simeq \frac{\gamma}{-\dot{\gamma}_{IC}} \simeq \frac{8 \cdot 10^{19} \text{ s}}{\gamma \, (1+z)^4} \approx 10^{14} s \approx 3.1 millon \ yrs \qquad \text{for } \gamma = 10^6 \tag{2.23}$$

A quick estimation of the distance of 1ES1218+30.4 (z=0.18) helps to understand the scale. z=0.18 corresponds to a distance of 2.46 Giga light years. Thus the IC scattering takes very little time in the propagation of a photon.

Notice the photon energy and the flux are always in redshift-zero units. Therefore the short lifetime of the electrons implies we can treat them this way as well. Since the IC energy losses are much faster than the cosmological expansion, we can therefore neglect the cosmological redshift for the electrons. To calculate how the IC losses modifying the spectrum of newly produced electron/positron pairs, we consider a balance equation

$$\frac{\partial}{\partial t} N(\gamma) + \frac{\partial}{\partial \gamma} (\dot{\gamma}_{IC} N(\gamma)) = Q(\gamma, t) \tag{2.24}$$

One thing to notice here is,the fully written balance function is

$$\frac{\partial}{\partial t} N(\gamma) + \frac{\partial}{\partial \gamma} (\dot{\gamma}_{IC} N(\gamma)) + \frac{N(\gamma)}{T(\gamma)} = Q(\gamma, t) \tag{2.25}$$

we ignored the third term on left handside because the decay term can be related with timescale

$$T(\gamma) = \frac{1+z}{3} \frac{dt}{dz} \simeq H_0^{-1} \simeq 4 \cdot 10^{17} \text{ s} \gg \tau_{IC} \tag{2.26}$$

so we can neglect also the volume effect of cosmological expansion.

Green's function for the time-dependent continuity equation (eq.17) with boundary condition $G(t = -\infty) = 0$ is

$$G = \delta\left(t - t' - \int_{\gamma'}^{\gamma} \frac{du}{\dot{\gamma}(u)}\right) \frac{1}{|\dot{\gamma}_{IC}|} \Theta\left(\frac{\gamma - \gamma'}{\mathrm{sgn}(\dot{\gamma})}\right) \tag{2.27}$$

We then have to solve

$$N(\gamma, z_b(i-1)) = \int^{t_{i-1}} dt' \int d\gamma' \, G(t', \gamma') \, Q \tag{2.28}$$

that is,

$$N(\gamma, z_b(i-1)) = \frac{1}{|\dot{\gamma}_{IC}|} \int^{t_{i-1}} dt' \int_{\gamma} d\gamma' \, \delta\left(t_{i-1} - t' - \int_{\gamma'}^{\gamma} \frac{du}{\dot{\gamma}(u)}\right) Q \tag{2.29}$$

With the source function as (with $t_i = t(z_b(i))$)

$$Q(\gamma, z_b(i-1)) = \frac{\delta N_e(\gamma', z_c(i))}{\delta z \, |\frac{dt}{dz}|} \Theta\left[t' - t_i\right] + N(\gamma', z_b(i)) \, \delta\left[t' - t_i\right] \tag{2.30}$$

with the first term as newly generated electron/positron pairs in current redshift bin and second term as the flux left over from previous bins. The first term in source function gives

$$N(\gamma, z_b(i-1)) = \frac{1}{|\dot{\gamma}_{IC}|} \int_{\gamma} d\gamma' \frac{\delta N_e(\gamma', z_c(i))}{\delta z \, |\frac{dt}{dz}|} \int_{t_i}^{t_{i-1}} dt' \delta\left(t_{(i-1)} - t' - \int_{\gamma'}^{\gamma} \frac{du}{\dot{\gamma}(u)}\right) \tag{2.31}$$

The delta function requires that

$$0 \leq \int_{\gamma'}^{\gamma} \frac{du}{\dot{\gamma}(u)} = \frac{1}{A\gamma} - \frac{1}{A\gamma'} \leq t_{i-1} - t_i = |\frac{dt}{dz}| \delta z \tag{2.32}$$

which leads to

$$\gamma'_{\max} = \begin{cases} \infty & \text{for} \quad A\gamma \frac{dt}{dz} \delta z \geq 1 \\ \frac{\gamma}{1 - A\gamma|\frac{dt}{dz}|\delta z} & \text{for} \quad A\gamma \frac{dt}{dz} \delta z \leq 1 \end{cases} \tag{2.33}$$

Therefore

$$N(\gamma, z_b(i-1)) = \frac{1}{A\gamma^2 \, \delta z} |\frac{dz}{dt}| \int_{\gamma}^{\gamma'_{max}} d\gamma' \, \delta N_e(\gamma', z_c(i)) \tag{2.34}$$

For the second term

$$N(\gamma, z_b(i-1)) = \frac{1}{|\dot{\gamma}_{IC}|} \int_\gamma d\gamma' N(\gamma', z_b(i)) \int^{t_{i-1}} dt' \, \delta\left(t_{i-1} - t' - \int_{\gamma'}^\gamma \frac{du}{\dot{\gamma}(u)}\right) \delta\left(t' - t_i\right) \quad (2.35)$$

since $t_i \leq t_{i-1}$, the delta function could be satisfied

$$N(\gamma, z_b(i-1)) = \frac{1}{|\dot{\gamma}_{IC}|} \int_\gamma d\gamma' N(\gamma', z_b(i)) \delta\left(t_{i-1} - t_i - \int_{\gamma'}^\gamma \frac{du}{\dot{\gamma}(u)}\right) \quad (2.36)$$

The delta function gives

$$\gamma'' = \frac{\gamma}{1 - A\gamma \left|\frac{dt}{dz}\right| \delta z} \quad (2.37)$$

$\gamma'' \geq 1$ so that

$$N(\gamma, z_b(i-1)) = \frac{1}{|\dot{\gamma}_{IC}|} N(\gamma'', z_b(i))$$

$$\gamma'' = \begin{cases} < 0 & \text{for} \quad A\gamma \frac{dt}{dz} \delta z \geq 1 \\ \frac{\gamma}{1 - A\gamma \left|\frac{dt}{dz}\right| \delta z} & \text{for} \quad A\gamma \frac{dt}{dz} \delta z \leq 1 \end{cases} \quad (2.38)$$

Therefore in total, for $A\gamma \left|\frac{dt}{dz}\right| \delta z \geq 1$

$$N(\gamma, z_b(i-1)) = \frac{1}{A\gamma^2 \delta z} \left|\frac{dz}{dt}\right| \int_\gamma^\infty d\gamma' \, \delta N_e(\gamma', z_c(i)) \quad (2.39)$$

for $A\gamma \left|\frac{dt}{dz}\right| \delta z \leq 1$

$$N(\gamma, z_b(i-1)) = \frac{1}{A\gamma^2 \delta z} \left|\frac{dz}{dt}\right| \int_\gamma^{\gamma'_{max}} d\gamma' \, \delta N_e(\gamma', z_c(i)) + \frac{N(\gamma'_{max}, z_b(i))}{(1 - A\gamma \left|\frac{dt}{dz}\right| \delta z)^2} \quad (2.40)$$

with

$$\gamma'_{max} = \frac{\gamma}{1 - A\gamma \left|\frac{dt}{dz}\right| \delta z} \quad (2.41)$$

2.4 Deflection of the electrons

During the calculation of absorption we ignored the change in direction of the produced electrons relative to the incoming gamma ray. There are two sources of misdirection:

1) The CM frame moves not exactly in the same direction as the incoming gamma ray. The combined momentum vector has a magnitude $E_\gamma (1 + z)$ in parallel direction and $\epsilon \sqrt{2x - x^2}$ in perpendicular direction. The ratio of the two is the sine of the angular kick

$$\sin \delta\theta \simeq \delta\theta \simeq \frac{\epsilon}{E_\gamma} \simeq 10^{-12}$$

which is safely ignorable.

2) The electron or positron is emitted in arbitrary direction in the CM frame, and therefore its direction in the Lab frame is aligned with that of the CM frame to the order $\delta\theta \simeq 1/\gamma_{\rm CM} \simeq 10^{-6} \simeq 0.1''$, significantly larger than calculated under point 1). While that displacement is not directly observable on account of the limited angular resolution of gamma-ray measurements, it may impose a time delay. The light travel-time difference between going straight and at an angle $\delta\theta$ over a distance L is

$$\delta t = \frac{L}{c}\left(\frac{1}{\cos\delta\theta} - 1\right) \simeq \frac{L}{2\,c}\,(\delta\theta)^2 \simeq \frac{z}{2\,H_0}\,(\delta\theta)^2 \simeq (2.5\ \text{days})\,z$$

Clearly, this is an issue when discussing rapid variability, but we can ignore it for time-integrated spectra, e.g. when analyzing VERITAS data taken over many nights.

Further calculation of the time delay goes as follows: Starting from the source, a photon will travel straight for a length ϵL, then almost immediately be turned into a photon of lower energy and deflected by some small angle θ, and then again straight for length $(1 - \epsilon)\,L$. Here we assume that no further absorption takes place, but that is probably fine because the secondary gamma ray produced in a second absorption event is almost certainly below 10 GeV. The cascaded photon has now traveled a total distance L, but is separated from the source by $L' < L$. The small difference is:

$$
\begin{aligned}
\delta L &= L - L' \\
&= L \times \left(1 - \sqrt{\epsilon^2 + (1-\epsilon)^2 + 2\,\epsilon\,(1-\epsilon)\,\cos\delta\theta}\right)
\end{aligned}
\tag{2.42}
$$

And the corresponding time delay is

$$
\begin{aligned}
\delta t &= \frac{\delta L}{c} \\
&= \frac{L}{c}\left(1 - \sqrt{\epsilon^2 + (1-\epsilon)^2 + 2\,\epsilon\,(1-\epsilon)\,\cos\delta\theta}\right) \\
&= \frac{z}{H_0}\left(1 - \sqrt{\epsilon^2 + (1-\epsilon)^2 + 2\,\epsilon\,(1-\epsilon)\,\cos\delta\theta}\right) \\
&\simeq \frac{z}{H_0}\left(1 - \sqrt{\epsilon^2 + (1-\epsilon)^2 + 2\,\epsilon\,(1-\epsilon)\,(1 - \frac{\delta\theta^2}{2})}\right) \\
&= \frac{z}{2H_0}\,\epsilon\,(1-\epsilon)\,\delta\theta^2 \\
&\simeq \epsilon\,(1-\epsilon) \times 2.5\,days
\end{aligned}
\tag{2.43}
$$

Time delay disappears when $\epsilon = 0$ or $\epsilon = 1$, corresponding to absorption at the source or at the observer location. Thus for a highly energetic photon ($\sim 10 TeV$), it is more likely to be absorbed close to the source, which slightly reduces the time delay. This is the reason why we collect more information from the high energies than low energies and get a 100 GeV peak in observation.

When electrons generated from the process of absorption propagate, they will be affected by the background magnetic fields and deflected by certain angle. A detailed analysis of deflection goes as follows. If the electron sees a constant perpendicular magnetic field for a pathlength λ, its deflection scales with its Larmor radius and is approximately

$$\delta\theta = \frac{\lambda}{r_L} = \frac{\lambda}{1.6 \cdot 10^{15} \text{ cm}} \gamma^{-1} \left(\frac{B}{\text{pG}}\right) \tag{2.44}$$

The distance the electron travels before it has lost most of its energy by radiation is given by

$$L_{\text{IC}} = c\,\tau_{\text{IC}} \simeq (3 \cdot 10^{30} \text{ cm}) \frac{1}{\gamma\,(1+z)^4} \tag{2.45}$$

There are $N = L_{\text{IC}}/\lambda$ individual sections with random direction of scattering, and therefore the total angular displacement is

$$\begin{aligned}
\delta\theta_{\text{tot}} \simeq \sqrt{N}\,\delta\theta \quad &\simeq \frac{\sqrt{L_{\text{IC}}\,\lambda}}{1.6 \cdot 10^{15} \text{ cm}} \gamma^{-1} \left(\frac{B}{\text{pG}}\right) \\
&\simeq \frac{0.07}{(1+z)^2} \left(\frac{\lambda}{\text{pc}}\right)^{0.5} \left(\frac{\gamma}{10^7}\right)^{-1.5} \left(\frac{B}{\text{pG}}\right)
\end{aligned} \tag{2.46}$$

We estimated before that a displacement of the order 10^{-6} only provides a light-travel delay of the order of a day and hence may be ignorable if we discuss TeV-band data combined from different nights.

If we concentrate on gamma-ray energies higher than 100 GeV, then upscattering of CMB photons (10^{-3} eV) requires $\gamma \simeq 10^7$, which would result from the absorption of a 10-TeV gamma ray. Using a Lorentz factor $\gamma = 10^7$ would then be fine, and an ignorable total deflection would require

$$\delta\theta_{\text{tot}} \le 10^{-6} \quad \Rightarrow \quad B \le (0.02 \text{ fG}) \left(\frac{\lambda}{\text{pc}}\right)^{-0.5} \tag{2.47}$$

This magnetic field is of the same magnitude as what is expected for cosmological seed fields, that is magnetic field prior compression by structure formation and associated shocks. We

expect that field to exist in the voids of the cosmological matter distribution, whereas in the filaments the field is expected to be much stronger.

However not all gamma rays are absorbed sufficiently far from the AGN that we can assume we are inside a void and magnetic field is ignorable. The spectrum and the flux level of the reprocessed emission could be greatly dependent on the intensity of the intergalacticmagnetic field, B. But under the assumption that the magnetic field is small and as long as we are talking about highly energetic photons, to ignore deflection is safe.

2.5   Inverse-Compton Scattering

The gamma-ray beam from the jets of AGN is highly anisotropic. Jets from AGN are low relativistic, with $\gamma \sim 15$ and thus the beam is open for about $2 \sim 3$ degrees. However the gamma-ray photons, the TeV emissions from jets are high relativistic. The energy range we consider is 100GeV-40TeV, with $\gamma \sim 10^6$, corresponding to deflection $\sim \frac{1}{\gamma} = 10^{-6}$. Therefore even with deflection we can observe only gamma-rays from a tiny section of the gamma-ray beam. we can use the cross section for isotropic electrons

$$\frac{d\sigma}{dE} = \frac{3\,\sigma_T}{4\,\epsilon_{\mathrm{CMB}}\,\gamma^2} \left[2\,q\,\ln q + (1+2\,q)(1-q) + \frac{(\Gamma\,q)^2\,(1-q)}{2\,(1+\Gamma\,q)} \right] \tag{2.48}$$

where E is the energy of the gamma ray produced and

$$\Gamma = \frac{4\,\epsilon_{\mathrm{CMB}}\,\gamma}{m_e\,c^2} \qquad 1 \geq q = \frac{E}{\Gamma\,(\gamma\,m_e\,c^2 - E)} > \frac{1}{4\,\gamma^2}$$

The major background light that would interact with our energy range would be 10^{-5} eV to several eV, that is CMB and EBL in the optical/near-IR. The blackbody spectrum of CMB is

$$n_{\mathrm{CMB}}(\epsilon) = \frac{dn}{dV\,d\epsilon} = (1+z)^3\,\frac{8\pi\,\epsilon^2}{h^3\,c^3}\,\frac{1}{\exp\left(\frac{\epsilon}{kT(1+z)}\right) - 1} \tag{2.49}$$

The increment in the gamma-ray spectrum on account of inverse-Compton scattering is

$$\delta F(E, z_c) = c\,\frac{dt}{dz}\,\delta z \int_{\gamma_{\min}} d\gamma\,N(\gamma, z_c) \int d\epsilon\,n_{\mathrm{CMB}}(\epsilon)\,\frac{d\sigma}{dE} \tag{2.50}$$

where $n_{\mathrm{CMB}}(\epsilon)$ is the blackbody spectrum of the CMB and

$$\gamma_{\min} = \frac{1}{2}\,\frac{E}{m_e\,c^2} + \sqrt{\left(\frac{E}{m_e\,c^2}\right)^2 + \frac{E}{\epsilon_{\mathrm{CMB}}}} \tag{2.51}$$

2.6 Updating the gamma-ray spectrum

Equation (2.7) now needs to contain a term the gains arising from Inverse-Compton scattering.

$$F(E_\gamma, z_b(i-1)) \simeq F(E_\gamma, z_b(i)) \ (1 - \delta\tau \left[z_c(i)\right]) + \delta F(E_\gamma, z_c) \qquad (2.52)$$

Gamma-ray spectrum is updated in each bin after IC radiation. In this way the newly generated secondary gamma-ray in each bin is thrown into the pool and takes part in the following steps.

CHAPTER 3.   INPUTS

3.1   Extragalactic Background Light

The EBL intensity originates from star and galaxy at optical, ultraviolet, and near-infrared wavelengths and reradiated thermal dust emission in far-infrared band in galaxies. Hence, the EBL is closely connected to the evolution with cosmic time of structure in the universe. However, the nature of major contributors to the EBL is largely uncertain (e.g., the evolution of the cosmic star formation rate;the amount of UV radiation from young, massive stars that escapes from the surrounding gas; the amount of re-emission by dust in galaxies). Furthermore, observations are hindered by emission from our own galaxy and the solar system. Nevertheless, despite the degree of complication, there are several approaches to overcoming the observational and theoretical uncertainties and, ultimately, modeling the EBL. We adopted one of them that is representative of the current state of field: the Franceschini et al (2008) EBL model.

A plot of the model predictions for the differential photon proper number density in proper units shows in Fig. 1. The two galaxy emission peaks, due to photospheric stellar emission (rest energy 1 eV) and dust re-radiation emission (rest energy 0.01eV), are clearly apparent in the figure at three redshifts at photon energies of $\epsilon \sim 1$ and 0.01 eV. Another behavior of the spectral densities is that of an increase of the photon proper density with redshift due to the Hubble expansion. The effects of the different rates of cosmological evolution of the background sources are also evident in Fig. 1. The evolution of galaxy population emissivity is greater in the IR ($\epsilon < 0.2eV$) than in the optical/near-IR ($\epsilon > 0.2eV$), because photons are produced at larger redshifts in the IR and lower redshifts in the optical. This reflects the fact that there is a larger increase in the proper photon density with z in the IR and a lower one in the optical/near-IR. In the latter case, the density increase due to the expansion is almost
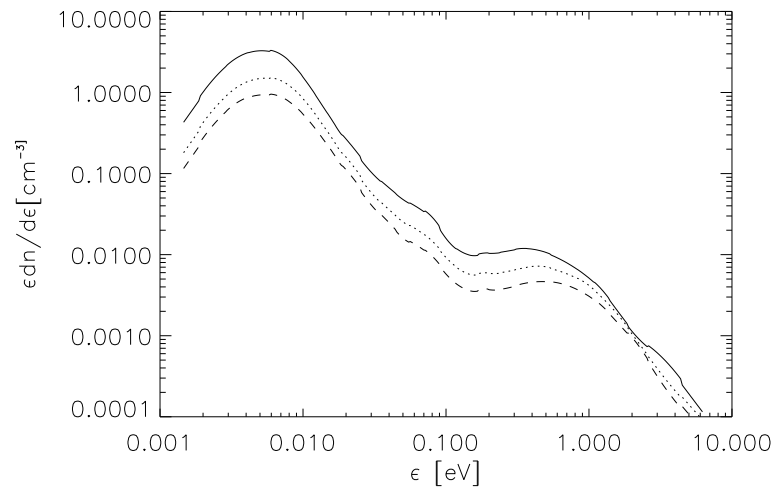
Figure 3.1   The redshift-dependent photon number density multiplied by the photon energy ϵ. Line in solid, dash-dotted and dash for source at redshift 0.6, 0.2, 0.
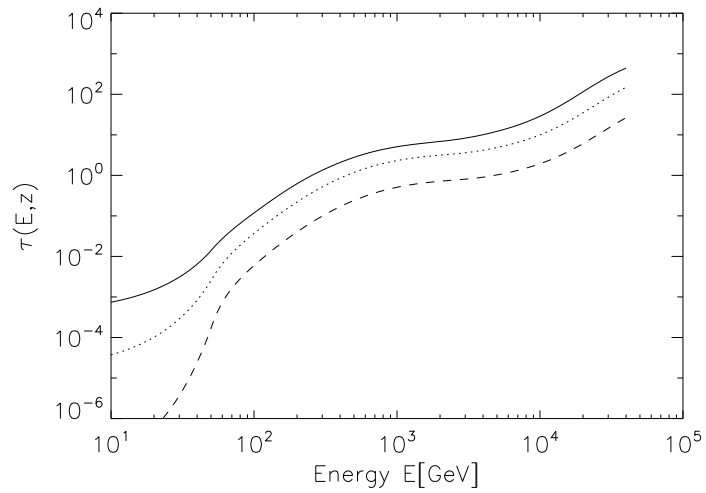

Figure 3.2   The optical depth by photon-photon collision as a function of the photon energy for sources located at redshift 0.4, 0.2, 0.05, from top to bottom.

compensated by the quick decrease with increasing z of the number of photons available.

The corresponding optical depth as a function of energy for sources located different redshifts is shown in Fig. 2. At redshift 0.2, optical depth is approximately 10^{-2} for 100GeV, 1 for 1TeV, 10 for 10TeV. Therefore we can expect that high energy band would be heavily absorbed while the shape of low energy band would be kept well since not much of it is lost during propagation. That is exactly what we see from observation-we can see a relatively high flux at GeV band but quite weak signals from TeV band.

CHAPTER 4.   RESULTS

4.1   Intrinsic spectrum of a sample blazar

To better illustrate our model, we first chose a sample blazar to demonstrate the result. We set the sample blazar to locate at z=0.536 and with observational spectral index of 1.80 between 0.2GeV and 300 GeV(FERMI range). The reasons we chose such a sample are as follows: on one hand, harder intrinsic spectral index helps to get more secondary photons involved; on the other hand, large redshift guarantees the TeV photons to interact completely.

A similar blazar that has been detected is 3C279, which also locates at z=0.536 but with index of 2.34 in this range. 3C279 is a prominent member of the class of active galactic nuclei (AGNs) containing super-massive black holes, typically a billion times more massive than the Sun, powered by accreting matter from surrounding stars or gas. The quasar's distance is more than five billion light years (roughly half the radius of the Universe) from the Earth, more than twice the distance of objects previously observed with this kind of radiation. AGNs emit radiation across the entire electromagnetic spectrum from radio wavelengths to very high energy (VHE) gamma-rays. 3C279 is one of the main targets of both MAGIC and FERMI. In FERMI catalog it is named after J1256.1-0548. It located at redshift 0.536 and with spectral index of 2.34 in FERMI range of 200MeV-300GeV.

Fig 4.1 and Fig 4.2 show the pictures of sample blazar by EGRET and MAGIC. Fig 4.3 and Fig 4.4 present our simulations of this blazar. The solid line in Fig 4.3 predicts the observed spectrum as a power law of $E_\gamma^{-1.8}$ in 10GeV-100GeV. The dash line is the intrinsic spectrum we used to generate the observed spectrum with index 1.8 in FERMI range and the original spectral index is 1.69.

As it is expected, the flux at high energies are greatly attenuated as a result of large optical
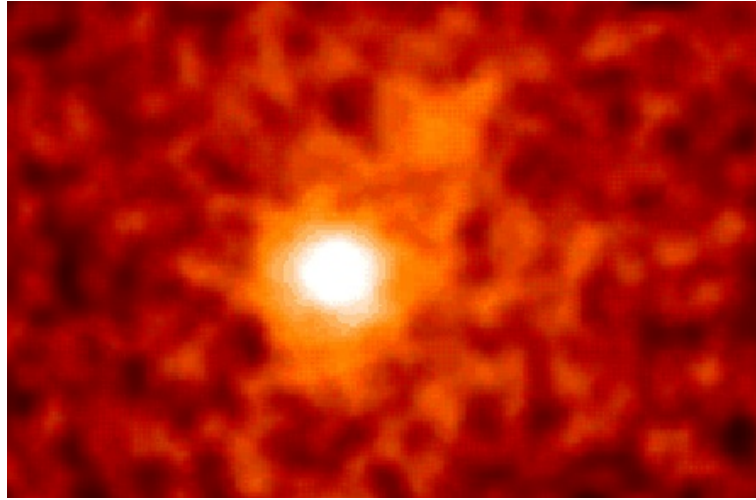
Figure 4.1   Picture courtesy APOD, EGRET team, Compton Observatory, NASA
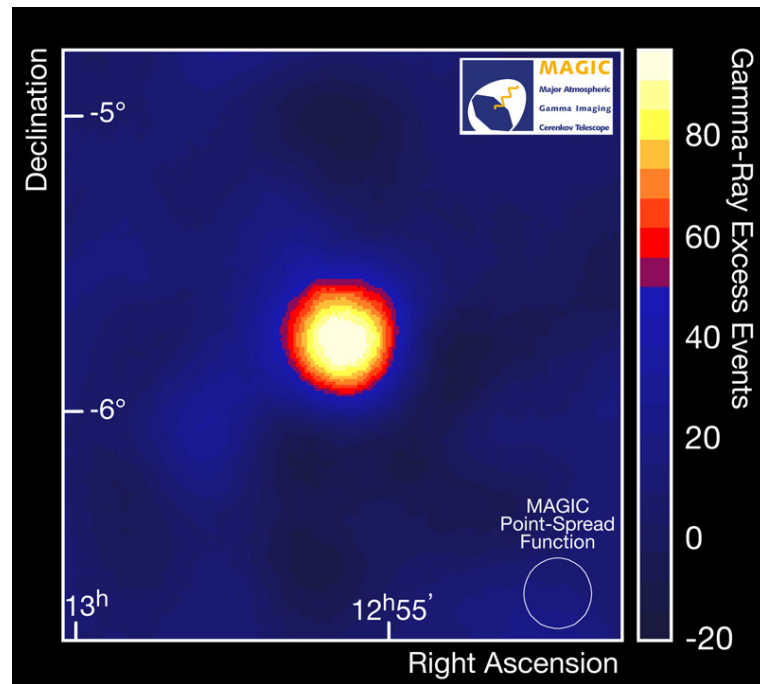

Figure 4.2   Sky Map of 3C279 in Very-High Energy photons as seen by MAGIC. The active galactic nucleus, from which these photons originated, is a quasar distant more than five billion light years from the Earth.
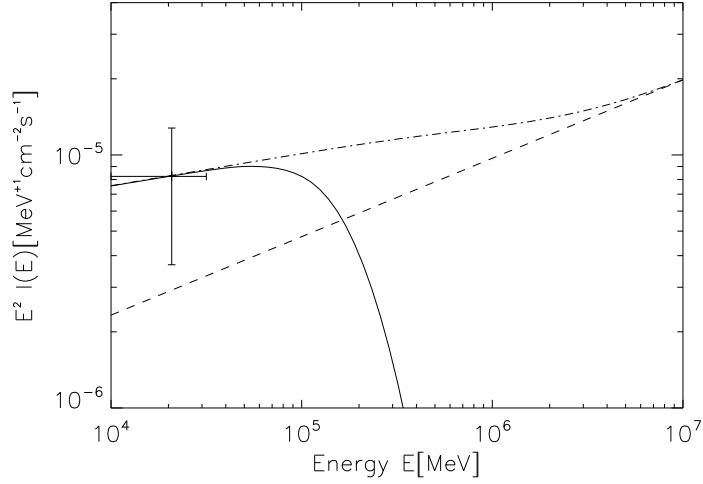
Figure 4.3   The EM cascade radiation from the propagation of VHE photons through the EBL. Solid line: prediction of observational blazar spectrum, with spectral index of 1.80 in 10GeV-100GeV. Dash line: the intrinsic spectrum at redshift 0.536, with spectral index of 1.69. Dash dotted line: the expectation source spectrum if only absorption but not EM cascade is accounted. Square date point: FERMI data for 3C279 with statistical and instrumental systematic uncertainties, used to scale the plot.

Figure 4.4   Comparison between spectrum with and without IC radiation. Solid: the blazar spectrum at $z = 0$ including both absorption and EM cascade. Dash: the blazar flux including absorption only.

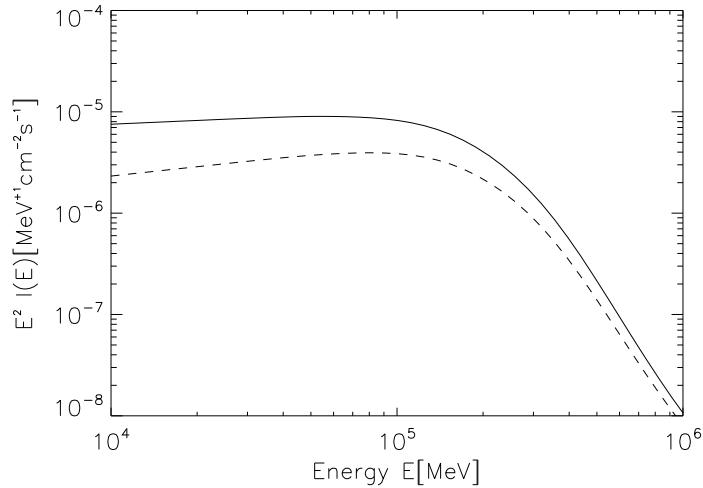depth thus deep absorptions there. However things become interesting at lower energies. The dash-dotted line is an expectation of source spectrum starting with observation data today and assuming there is only absorption. The difference between dash-dotted and solid lines presents the error it would have brought in if without considering IC process. As evident in Fig. 4.3, the amount of EM cascade created in the propagation of VHE photons can be substantial in 10-100GeV, the sensitive range of FERMI energy window. It happens so since the secondary gamma-ray flux generated by primary gamma-ray at TeV band would ultimately show up in 10-100GeV band. And the total amount of EM radiation is significant that it is about 4 times greater than the original spectra in that band. Hence by taking account the IC process, the intrinsic spectrum could be better predicted with observational data.

Further, Fig. 4.4 presents a comparison between total spectrum and the spectrum by absorption only. As shown in dash, without considering IC scattering, the observational data is an exponential curve tangential to the intrinsic spectrum at 10 GeV due to the fact that optical depth is quite small (to the order of 10^{-3}) there. The observed data including EM radiation turned out to be about 4 times greater and at the same time has a softer spectral index. Their difference goes lower in higher energies, and that is because optical depth becomes 3 orders larger and absorption behaves as the dominant factor.

One more interesting conclusion to point out here is our results predict harder spectrum than expected. The dash-dotted line in Fig 4.3 is nothing else but the prediction of intrinsic spectrum if consider absorption only. Since the optical depth for GeVs are sufficiently small, the expectation spectral index is therefore about the same value, like 1.80 here, as that of observation in 10-200GeV. Thus instead of a soft spectra with $\Gamma = 1.80$, our work including the flattening effect of EM cascades predicts a harder intrinsic spectral index of 1.69.

4.2   Test with VERITAS source - 1ES1218+304

1ES1218 is a typical TeV blazar at $z = 0.182$, with spectral index $\Gamma = 3.07 \pm 0.09$ in 200 GeV to 1.8 TeV. We start out with intrinsic spectral index of 1.68, which would practically generates an observational spectral index of 3.0. Fig 4.5 shows a prediction of the observation of
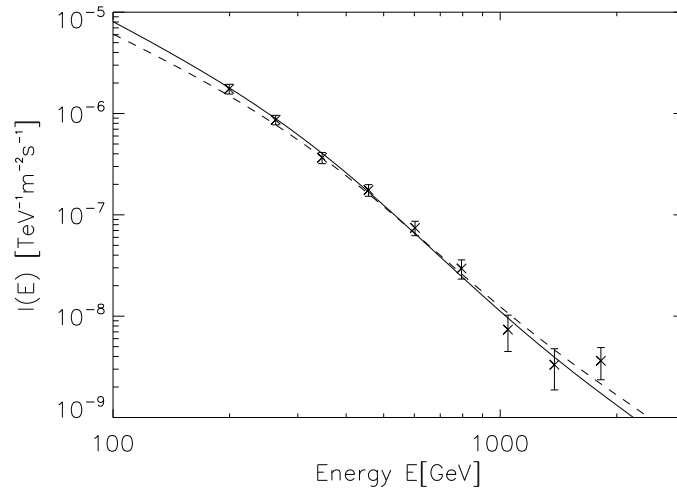
Figure 4.5   TeV spectrum of 1ES1218. Solid: the prediction of observed blazar spectrum. Dash: the prediction with same intrinsic spectral index but without IC radiation. Cross data points: the VERITAS observation data, based on an excess of 1155 events with a statistical significance of 21.8 standard deviations, σ, from the direction of 1ES 1218+304 during the 2008-2009 campaign (2808 signal events, 4959 background events with a normalization of 0.33).
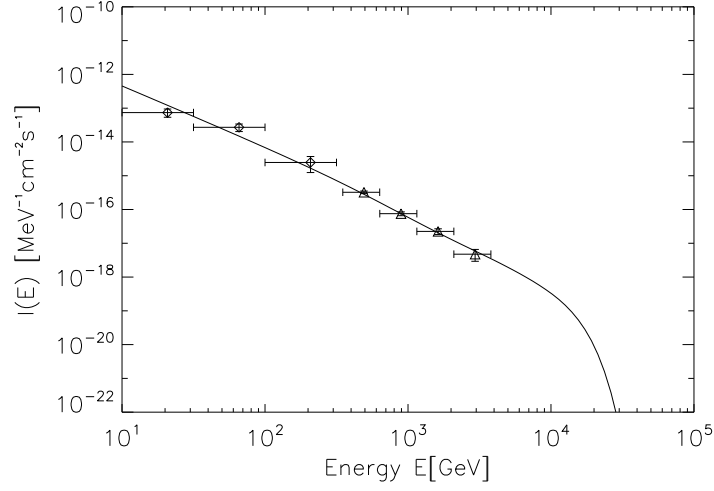
Figure 4.6   Test with J1104.5+3811. Dash: the prediction of observed
blazar spectrum. Square data points: the FERMI observation
data of J1104.5. Triangle data points: the MAGIC observation
data of M421.

1ES1218 (in solid and dash according to with/without cascade), comparing the real observation

data from VERITAS(in cross data points).

As presented in Fig 4.5, the prediction of the blazar 1ES1218+304 offered a decent match

with the observation by VERITAS around TeV bands. There is an upper trend at 400GeV

from the observation and this is clearly shown in the prediction curve. As a comparison,

the prediction from same spectral index but without cascade to result in a softer spectrum,

however gave a less plausible fit to the data. Hence the intrinsic spectral index predicted from

our theory is 1.68.

Moreover, previous work (Krennrich, F (2008)) showed that the differential spectral index of

the intrinsic spectrum of the three blazars J1218 is 1.28±0.20 or harder. We obtained 1.68 here

due to the different EBl model (we used the model from A. Franceschini (A. Franceschini.&

G. Rodighiero. (2008))).

redshift bin	energy transferred to e^- (%)	secondary γ-rays (%)
0.299	91.1	70
0.15	13.1	0.09

Table 4.1 Energy check. The first column is the redshift bin where we performed the check. The second is the fraction of the absorbed energy by e^- over the total energy. The third is the fraction of cascade radiation.

4.3 Test with FERMI and MAGIC source-Markarian 421

Markarian 421, named as J1104.5+3811 in the FERMI catalog, is a typical GeV blazar at $z = 0.03$, with spectral index $\Gamma = 1.86 \pm 0.02$. In calculation we took the intrinsic spectral index as 1.77, which will practically generates an observational spectral index of 1.86. Fig.4.6 shows a prediction of the observation of J1104.5(in dash), comparing the real observation data from FERMI(in square data points) and MAGIC(in triangle data points). The prediction goes through the error bars of the testing points and well matches the trend in which data preserve. It therefore can be concluded that our prediction satisfies the observational data from both FERMI and MAGIC for the source M421.

Notice here we did not use VERITAS or Whipple data because the flux from Markarian 421 is highly variable.

4.4 Energy check (source at 0.3)

We performed a check of the total energy in two scenarios to see how the energy evolves. The first is right after the pair production. We record the absorbed energy by electron and positron pairs. That is the second column in table 4.1.

$$E_1 = \int d\gamma \, \delta N_e(\gamma, z_b(i)) \, \gamma \, m_e \, c^2 \tag{4.1}$$

The second position we performed the check is after the IC radiation process. That is the third column in table 4.1.

$$E_2 = \int dE_\gamma \, \delta F \, E_\gamma^2 \tag{4.2}$$

The sample target we chose locates at $z = 0.3$ and has spectral index of $\Gamma = 1.8$.

We argue that the total energy should be conserved during each process, since theoretically there is no energy loss- all energy contained in primary gamma-rays would transfer to e^- through pair production, and this energy is passed to secondary gamma-rays in the later Inverse-Compton process. However in the simulation there is energy loss, depend on the redshift steps explicitly. This happens because secondary photons have much lower energy than the primary gamma-ray(about two decades lower), and the detectors (also our simulation) can only record a portion of the secondary photons that are above the threshold (10GeV in our code). The energy loss due to the neglect of lower end of spectrum becomes severe after about 0.1 redshift, corresponding to 1333 redshift bins, as a cumulative result of low energy cutoff. Also after one thousand steps, the high energies have almost gone due to the harsh absorption there and the flux peak has shifted to a few TeVs or even lower which produces a secondary peak beyond our record. This is shown in the second row of table 4.1, that after travelling for 0.15 redshift, the total energy is lost by a bad degree.

However the energy check near the source is satisfying. Our test result in first row of table 4.1 at redshift 0.299(10 steps from the source) preserves the total energy to a decent degree. Thus the check proves the simulation was efficiently operated and well explained.

CHAPTER 5.   SUMMARY AND DISCUSSION

We have analytically calculated the flux of gamma-rays undergoing pair production and Inverse-Compton scattering. We demonstrated the effects of EM cascades radiation on the contribution to the individual blazar spectra finding that the cascade radiation flattens the overall spectra and greatly enhanced the intensity at the high-end of the FERMI energy range. We have also shown that the amount of cascade radiation is sensitive to the optical depth and the nature of blazar spectra. We made use of the individual spectra as determined from the most recent data provided by FERMI and VERITAS testing the predictions of our code. Furthermore we have performed energy checks with our data and discussed the conservation of energy during the process.

As demonstrated in this thesis, EM cascades greatly enhances the flux of individual blazars and effectively flattens the spectrum in the observational regime. The overall spectrum generally has an exponential shape, resulting from the absorption by extragalactic background light via pair production. In advance, with the secondary gamma-rays coming from Inverse-Compton scattering with cosmic background light by primary gamma-rays with energy approximately one decade higher, EM cascades modify the spectrum by lifting and flattening the lower energies.

How much is flattened, that is, the difference between the intrinsic spectral index and observed spectral index is greatly dependent on redshift, intrinsic index and the energy range interested in. The contribution from EM cascades goes larger for farther objects. In our test the blazar M421 located in redshift 0.03 has a minor difference between spectrum with absorption only and with both EM cascades and absorption, comparing to the obvious difference in results of sample blazar which is much further with redshift 0.536. On one hand, optical depth goes

steeper as redshift grows, which means absorption is severer at larger redshifts. The high energy electron-positron pairs are the generators of the IC scattering. More absorption makes more IC scattering rounds and therefore more secondary gamma-ray. On the other hand, larger redshift corresponds to more steps in the code to reach the redshift 0. More secondary gamma-ray is taken into account by the code and thus the cumulative difference is more obvious.

The effect of EM cascades on observation spectrum is also related to the intrinsic spectral index of the individual blazar. In an energy flux-energy plot, harder blazars with spectral index less than 2 has positive slope. This means there is more energy distributed in high energy band than in low band for such blazars. Thus more high energy photons are able to participate in the cascading process and more radiation is generated. At the same time, these secondary photons are presented in the low energy band, which happen to be an initially weak background. As a result the effect of cascades runs obvious for hard blazars. However softer blazars which has spectral index larger than 2 would be in the other way. There is more energy located in the GeVs but less photons in TeVs that can generate electrons energetic enough to participate in IC scattering. The effect of EM cascades is weak in this situation.

A third factor that decides the effect of EM cascades is the energy range we look into. Photons in primary gamma-rays with TeV energy would ultimately generate most secondary gamma-rays in several hundreds GeV. A peak for secondary photons in several TeVs will ask for primary photons in over hundred TeVs, which is impossible due to the cutoff in high energy. Thus for most of the blazars, EM cascades effect shows up in 10-200GeV, which is also the FERMI range. If we look into the TeV band, the dominant effect there would still be the absorption by EBL. Like in our example of the VERITAS target 1ES1218, which was introduced in the TeV band, there is little difference between the spectrum considering absorption only and with both effects. If we prolonged the energy window wider, we would see a clearer difference there.

As noted in section 2.4, with negligible magnetic fields, the cascades are highly collimated in the direction of the propagating VHE photons. Thus the relativistic beaming of the intrinsic gamma-ray emission from AGNs ensures that observable gamma-rays originate only from those

AGNs that are favorably aligned with respect to the observer. In the presence of substantial magnetic fields, the cascades will no longer be collimated, which would also introduce halos of gamma-ray emission around blazars and contribute to source confusion. Also the presence of substantial magnetic fields would introduce a synchrotron component in the cascades redistributing the energy in the spectrum of cascade radiation.Synchrotron radiation is negligible until B is at μG level. Our current work does not count deflection. Besides the assumption of small magnetic fields, the effect of time delay in observation also provides reasons to neglect deflection. The deflection angle is proportional to the inverese of lorentz factor of the center momentum frame for electron-positron pairs, which is equal to half of the lorentz factor of main photons due to the symmetry. Thus the higher energy photons have, the smaller deflection angles there would be. On the other hand the delay time due to the deflection is proportional to inverse of the square of lorentz factor, and that means lower band would have more time delay. Our results show that the time delay is important. We see a 100GeV bump because we can record the IC radiation from high energies. The flux drops after about 100GeV since time delay is sufficient there and less information is recorded from the low energies. However one newly submitted paper (Tavecchio, F (2010)) represented that the implications for the source spectra argue against the existence of a cascading component and hence against very weak magnetic fields. More work will be done in the future to discuss the effects of deflection on propergation.

It should be noted that our theory tend to predict harder intrinsic spectral index. The cascading in a low-B environment makes the spectra below a certain energy softer, hence the intrinsic spectra must be harder to fit the same observed spectrum. Gamma-ray spectra of blazars with $\Gamma = 1.5$ were considered inconsistent with TeV spectra that originate from processes that involve diffusive shock acceleration (Krennrich, F (2008)). However in our work we show that due to the effect of EM cascades, the spectral index in observational energies is softer than the intrinsic spectral index. Take the sample blazar as an example, the intrinsic Γ is 1.69. But EM cascades effectively flattened the spectrum in the range of 100-200GeV, which resulted in an observational spectral index of 1.80 by FERMI (A. A. Abdo (2009)). But

if there was only absorption by EBL that affected the shape of spectrum, we would have 1.80 as the intrinsic spectral index in 10-200GeV since the optical depth there is sufficiently small. Thus given the same observation fact, we tend to predict harder intrinsic spectra as a result of the flattening effects from EM cascades. Some explanations of hard spectrum indicate that sufficiently hard electron spectra could be generated by diffuse shock acceleration at relativistic shocks. It is also indicated that a high low-energy cutoff in the electron distribution could give the appearance of a hard gamma-ray spectrum for a given energy regime. Aharonian (F.A.) show that absorption in the source due to narrow band emission from the AGN could lead to unusually hard TeV spectra from AGNs. On the other hand, hard spectrum allows us to derive a lower limit on the MF and talk about the relation to the 1-100 GeV extragalactic gamma-ray background.

Thus, the study of the individual blazar intensity, including the effects of cascade radiation, combined with the measurements of the VERITAS, FERMI can provide a wealth of insight into the nature and evolution of blazar spectra.

BIBLIOGRAPHY

A. A. Abdo, et al.(2009).The Spectral Energy Distribution of Fermi bright blazars *The Astrophysical Journal Letters*,

Aharonian, F.A. et al., (2008). Upper limits from HESS active galactic nuclei observations in 2005-2007 *Astronomy & Astrophysics*, *478*(387)

A. Franceschini. G. Rodighiero. etc. (2008). Extragalactic optical-infrared background radiation, its time evolution and the cosmic photon-photon opacity *Astronomy and Astrophysics* , *487*(3) pp.837-852

Krennrich, F., et al.(2008). Constraints on Energy Spectra of Blazars based on Recent EBL Limits from Galaxy Counts *The Astrophysical Journal Letters*, *689*(2)

Gould, R. J., & Schreder, G. (1966). *Phys. Rev. Lett.*, *16*(252)

Heitler, W., (1960), The Quantum Theory of Radiation, Oxford Press, London

Jones, F.C. (1963). The energy spectrum of galactic electrons produced by cosmic rays. *Journal of Geophysical Research (U.S.)*, *68*(4399)

F. Tavecchio, et al.(2010). The intergalactic magnetic field constrained by Fermi/LAT observations of the TeV blazar 1ES 0229+200. *Submitted to MNRAS (Letters)*,

Tonia M. Venters (2010). Contribution to the extragalactic gamma-ray background from the cascade of very-high energy gamma rays from blazars. *The Astrophysical Journal* , *710*(2)

Tonia M. Venters (2009). The Extragalactic background light absorption feature in the blazar component of the extragalactic gamma-ray background. *The Astrophysical Journal* , *703*(2)